Synthesis, Crystal Structure, and Photophysical and Magnetic Properties of Dimeric and Polymeric Lanthanide Complexes with Benzoic Acid and Its Derivatives

Alex Wai-Hing Lam,[a] Wing-Tak Wong,*[a,b] Song Gao,[b] Gehui Wen,[c] and Xi-Xiang Zhang[c]

Keywords: Carboxylate ligands / Lanthanides / Luminescence / Magnetic properties

A new family of lanthanide carboxylate complexes with benzoic acid and its derivatives was synthesised and characterised. The structures of the complexes were established by X-ray crystallography, which revealed that various chelating modes of the carboxylate ligands are present on the metal ion, resulting in the formation of dimeric and polymeric skeletons. The photophysical properties of the Eu and Tb complexes were studied: the complexes exhibited sensitised luminescence in the visible spectral region, but the luminescence intensities and lifetimes were very sensitive to quenching by the OH groups of methanol molecules. The solid-state magnetic properties of the Gd and Tb complexes demonstrated the presence of weak antiferromagnetic exchange interactions at very low temperatures, caused by interaction between the neighbouring ions along the chain.

(© Wiley-VCH Verlag GmbH, 69451 Weinheim, Germany, 2003)

Introduction

The design of molecular systems that combine binding abilities and photosensitising properties for the construction of efficient photoluminescent lanthanide complexes continues to be an active area of research. Several classes of ligand have been utilised for the preparation of such complexes; they include cryptands,[1] podands,[2] calixarenes,[3] macrocyclic ligands,[4] β-diketones,[5] carboxylic acid derivatives,[6] terphenyl ligands,[7] and proteins.[8] Most of the complexes investigated emit red or green light (Eu^{3+} and Tb^{3+} luminescence, respectively), but there are also complexes of different Ln^{3+} ions that luminesce in other spectral regions. Efficient luminescent materials may have several applications: as luminescent probes in biomedical assays,[9] as luminescent sensors for chemical species (H^+, O_2, halide ions, OH^-),[4c] and as electroluminescent devices,[10] for example. Besides the quantum yield of the luminescent lanthanide materials, other aspects such as light output, solubility, volatility, and photo-, thermo- and thermodynamic stabilities may be critical to many applications, and must also be controlled.

Variation of the coordination geometries of the central metal atom, and also of the carboxylate ions in the lanthanide carboxylate complexes, are interesting themes of structural chemistry.[11] Over the past twenty years, many structural studies of lanthanide carboxylates have been reported, and diverse coordination types recognised. A large number of lanthanide carboxylate complexes have been found to be dimeric or polymeric.[11a] A one-dimensional system is believed to impose the greatest restriction on metal−metal interaction, and energy migration that depends on such interaction between nearest neighbours in the lattice will thus be dominant in the chain direction. Research studies on polynuclear lanthanide complexes may therefore provide information concerning exchange and magnetic interaction mechanisms. Numerous aromatic carboxylic acids of europium and terbium are chelated in binary or ternary fashion and exhibit high stability and strong luminescence. Tb^{3+} luminescence is enhanced by more than 10^4-fold by dipicolinic acid, and Eu^{3+} luminescence is similarly enhanced by diketonates. The common feature for strong sensitisation is the direct coordination of a conjugated π-electron system to the metal ions. Photoluminescence properties notwithstanding, several studies have demonstrated that luminescent lanthanide complexes have potential for application as emitters in electroluminescent (EL) devices.[12] Kido et al.[13] reported organic electroluminescent devices based on trivalent terbium or europium complexes with β-diketones.

[a] Department of Chemistry, The University of Hong Kong, Pokfulam Road, Hong Kong, P. R. China,
Fax: (internat.) + 852/25472933 or 28571586
[b] PKU-HKU Joint Laboratory on Rare Earth Materials and Bioinorganic Chemistry, Peking University, Beijing 100871, P. R. China
[c] Department of Physics, Hong Kong University of Science and Technology, Clear Water Bay, Kowloon, Hong Kong, P. R. China

Supporting information for this article is available on the WWW under http://www.eurjic.org or from the author.

However, these complexes were limited by their poor photostabilities. As complexes with unlimited polymeric chain structures, lanthanide carboxylates have not only good luminescent properties, but also good ultraviolet absorption properties. Some representative examples of lanthanide carboxylate complexes that can be fabricated as EL devices are $[Tb(AHB)_3]$ (AHBA = 2-amino-4-hexadecylbenzoic acid),[14] $[Tb(MeOBB)_3]$ and $[Eu(MeOBB)_3]$ [MeOBB = 2-(4-methoxybenzoyl)benzoic acid].[15]

In view of the potential applications of lanthanide carboxylates and the fascinating properties of carboxylate ligands, a new series of lanthanide carboxylate complexes (Eu, Gd, and Tb) with benzoic acid and its derivatives were synthesised: $[Ln_2(Bz)_6(MeOH)_4]_n$ (**1a**−**c**), $[Ln(Bz)_3(DMF)]_n$ (**2a**−**c**) (HBz = benzoic acid), $[Ln(cf_3)_3(MeOH)_2]_n$ (**3a**−**c**) (Hcf_3 = 4-trifluoromethylbenzoic acid), $[Ln(ocf_3)_3(MeOH)_2]_n$ (**4a**−**c**) ($Hocf_3$ = 4-trifluoromethoxybenzoic acid), $[Ln(oet)_3(DMF)(H_2O)]_2$ (**5a**−**c**) (Hoet = 4-ethoxybenzoic acid), and $[Ln(opr)_2(NO_3)(MeOH)_2]_n$ (**6a**−**c**) (Hopr = 4-*n*-propoxybenzoic acid). Their structures demonstrate the rich coordination chemistry of lanthanide carboxylate complexes, and the structures of Eu, Gd and Tb complexes with the same ligand are isomorphous. The luminescent and magnetic properties of these lanthanide complexes have also been studied and are discussed.

Results and Discussion

Syntheses and Crystal Structures of Lanthanide Complexes

Treatment of hydrated lanthanide (Eu, Gd, and Tb) nitrates with NaOH and the corresponding benzoic acid ligands in MeOH (1:3:3 ratio) afforded precipitates of the complexes (Scheme 1). The complexation of the lanthanide complexes was confirmed by IR spectroscopy, the absence of ν(COOH) absorption bands of the ligands at about 1700 cm^{-1} in all spectra indicating the coordination of ligands to the metal. All the IR spectra show the presence of absorption bands characteristic of the carboxylate groups. The bands at about 1600−1500 cm^{-1} correspond to the asymmetric vibrations of COO^- groups, while those at about 1450−1350 cm^{-1} are attributable to their symmetric vibrations. Several $\nu(COO^-)_{as}$ bands suggest that different coordination modes of carboxylate groups are present in the complexes, as is confirmed by structural analyses. Complexes with coordinated MeOH molecules exhibited a broad

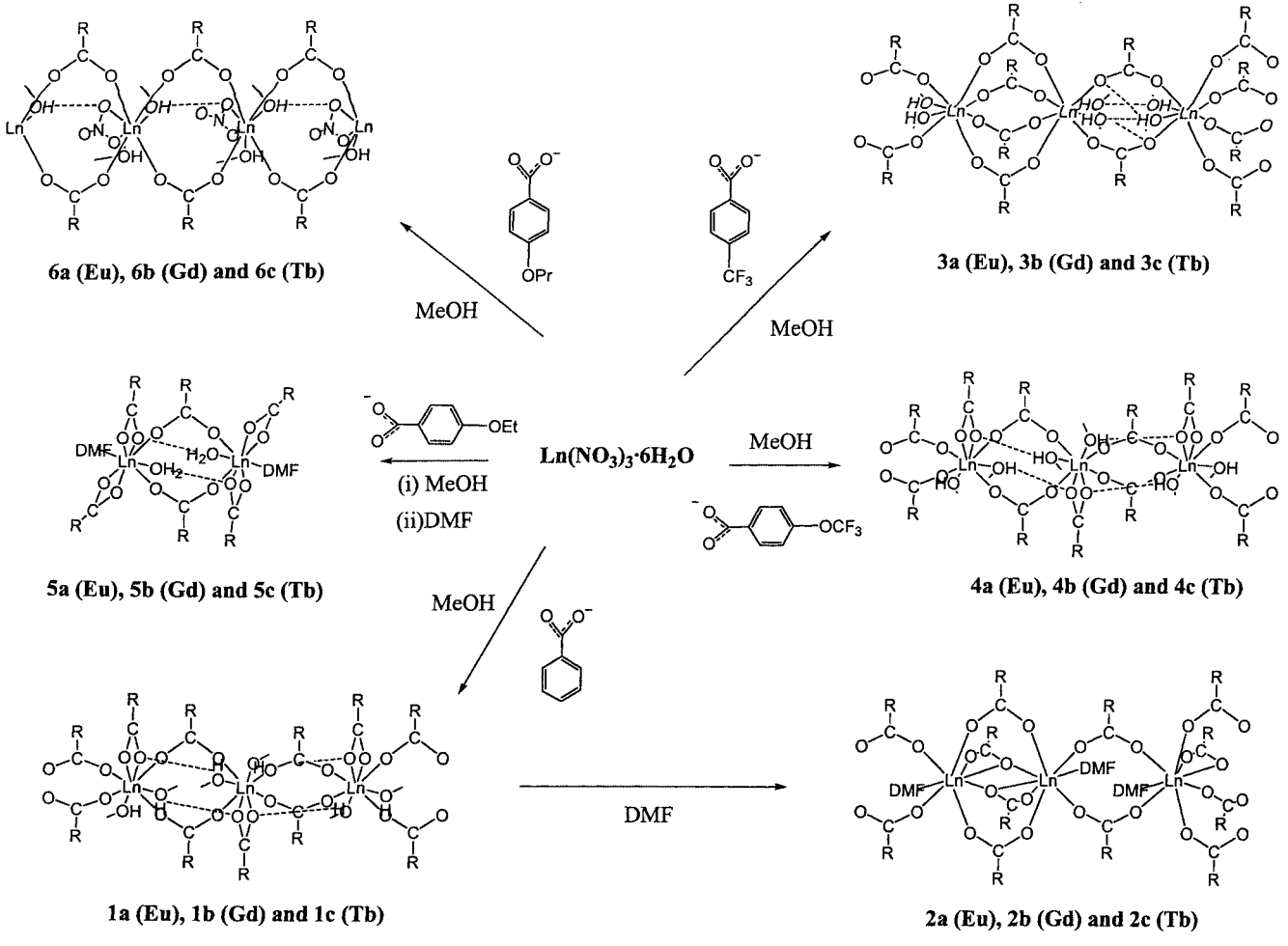

Scheme 1

ν(O−H) band at about 3500 cm^{-1}, and those complexes containing the fluorinated benzoate ligands showed the corresponding ν(C−F) stretching range from 1300 to 1100 cm^{-1}. The presence of absorption bands at about 1660 cm^{-1} is attributable to the ν(C=O) of the DMF molecule, which confirms the successful replacement of MeOH by DMF molecules in complexes **2a**−**c** and **5a**−**c**. According to the ESI-MS studies of the complexes, a series of characteristic peaks were observed, the most intense peaks corresponding to the formulation of anionic fragments being $[LnL_4]^-$ and $[Ln_2L_7]^-$, where L is the respective benzoate ligand. This observation revealed that dimeric or oligomeric complexes would retain their dimeric/oligomeric natures in solution. The thermal decomposition behaviour of the complexes was investigated by a TGA study, although no attempt was made to identify the intermediate products formed during this thermolysis. The first step in the thermogram corresponds to the distinct loss of coordinated solvent molecules [MeOH (ca. 30−120 °C) or DMF (ca. 100−160 °C)], in line with their X-ray crystallographic results. The total weight losses are compatible with the formulas, and the masses of the final products correspond to the complete combustion of the complexes to their corresponding oxides (Eu_2O_3, Gd_2O_3, Tb_2O_3, or Tb_4O_7) at 900 °C.

Single crystals of complexes **1a**−**c**, **2a**−**c**, **3a**, **3c**, **4a**−**c**, **5b**, **5c**, and **6c** were obtained by slow evaporation of their corresponding solvents for a period of time, and their structures were established by X-ray crystallography. Structures of complexes (Eu, Gd, and Tb) with a particular ligand are isostructural, so a detailed structural description of the complexes is exemplified by one of them.

The polymeric structure of complex **1a** is displayed in Figure 1, and selected bond lengths and bond angles are given in Table 1. This analysis revealed that there are two independent and distinct Eu^{3+} ions, bridged through four ligand carboxylate groups to form an infinite chain along the *a* axis. Each Eu^{3+} ion is coordinated by two O atoms from a bidentate chelating carboxylate group, four from four different ligands in a bridging mode, and two O atoms from two methanol molecules. Along the chain, the metal−metal distances and angle are: Eu(1)···Eu(2) = 4.90 Å, Eu(1)···Eu(2*) = 4.93 Å and Eu(2*)−Eu(1)−Eu(2) = 165.7°. The coordination geometry around the Eu(1) atom can be described as a distorted square antiprism, in which the top square face is defined by O(2), O(4), O(5), and O(14), and the bottom one is formed by O(6), O(7), O(9), and O(13). The dihedral angle between the square faces is 9.16°. Meanwhile, the geometry of the Eu(1) atom can also be described as a distorted bicapped trigonal prism, in which the top plane is defined by O(2), O(5), and O(7), and the bottom plane is completed by O(4), O(9), and O(14). The O(6) and O(13) atoms cap two quadrilateral faces of the trigonal prism. The dihedral angle between the planes is 10.35°. This observation of coordination polyhedra also applies for the Eu(2) atom, which can be described as a distorted square antiprism or a bicapped trigonal prism. The dihedral angles between the square and the trigonal planes are 8.55 and 12.17°, respectively. The Eu−O bond lengths range from 2.309(6) to 2.535(6) Å for both Eu^{3+} ions. The Eu−O(CO) carboxylate bond lengths of the bidentate chelating species [2.468(6)−2.527(6) Å] are longer than those of the bridging one [2.309(6)−2.367(6) Å], due to the formation of an unstable four-membered ring.[16] The Eu−O(MeOH) distances range from 2.496(6) to 2.537(6) Å. Intra-chain hydrogen bonding is observed between the methanol H atoms and the carboxylate O atoms [O(13)···O(11) = 2.72 Å, O(14)···O(12*) = 2.83 Å, O(15)···O(5*) = 2.76 Å, O(16)···O(6) = 2.82 Å]. Although the methanol H atoms could not be located, an analysis of the spatial relationships of the proximal potential donors and acceptors indicated an unambiguous pattern for the hydrogen bonding interactions. This type of coordination mode of ligands has been observed in the complex $\{[Eu(\alpha\text{-}C_5H_3O_3)_3(H_2O)_2]\cdot NO_3(4,4'\text{-Hbpy})\}_n$.[17]

A perspective view of the polymeric structure of complex **2a** is shown in Figure 2 and selected bond lengths and bond angles are summarised in Table 2. The structure demonstrates that each Eu^{3+} ion is connected to two neighbouring ones by six ligands through the carboxylate groups, to form an endless polymer. The carboxylate groups of the six molecules of benzoate are bidentate bridging and tridentate chelating-bridging. Four of the six carboxylate groups simultaneously bridge two Eu^{3+} ions, while the other two carboxylate groups chelate one Eu^{3+} ion and at the same time bridge two Eu^{3+} ions. Each Eu^{3+} ion is further coordinated to one DMF molecule to form eight-coordinate metal ions. The intra-chain Eu···Eu distances within the structure are Eu(1)···Eu(1*) = 3.93 Å and Eu(1)···Eu(1′) = 5.34 Å. The angle Eu(1′)−Eu(1)−Eu(1*) is 169.5°, and we can regard this as a linear chain along the *c* axis. The alternating metal−metal distances along the chain can be explained by the chelating-bridging carboxylate groups linking the Eu^{3+} ions, which result in shorter Eu···Eu distances than seen in other polymeric lanthanide carboxylates.[18] In addition, the larger steric effect of DMF relative to MeOH may cause the lengthening of the Eu···Eu distances; a similar observation has been noted in the Eu^{3+} complex with *N*-methylglycine.[19] The Eu−O(CO) bond lengths of bidentate bridging carboxylate groups [2.306(3)−2.403(3) Å] are smaller than those of the tridentate chelating-bridging moieties [2.333(3)−2.580(3) Å].

A crystal of complex **3a** suitable for X-ray analysis was sealed in a capillary and the molecular structure was established by X-ray crystallography. As illustrated in Figure 3, the Eu^{3+} ion in complex **3a** is coordinated by eight oxygen atoms, six of which [O(1), O(2), O(3), O(4*), O(5), and O(6)] are from six different carboxylate groups, while the other two [O(7) and O(8)] are from two coordinated methanol molecules. The Eu(1) atom is connected to two neighbouring Eu atoms [Eu(1′), Eu(1*)] alternatively by two bridging carboxylate groups and by four bridging carboxylate groups, to form an infinite one-dimensional chain along the *a* axis. Thus, along the chain, the Eu···Eu distances in the complex are alternatively long [Eu(1)···Eu(1′) = 5.42 Å] and short [Eu(1)···Eu(1*) = 4.19 Å]. With the alternating Eu···Eu distances and the chain

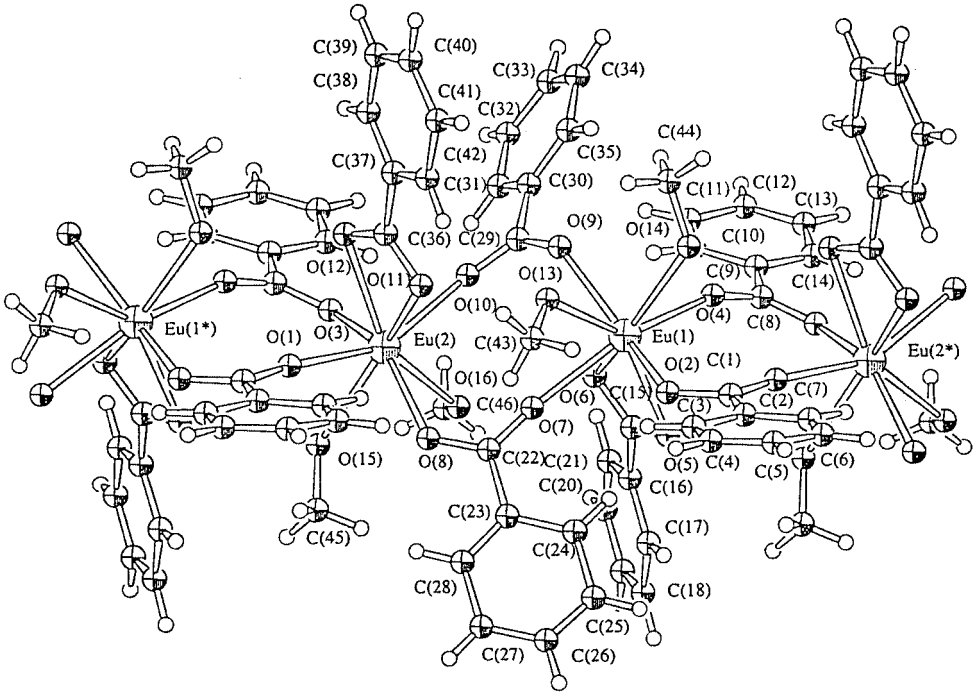

Figure 1. Polymeric structure of $[Eu_2(Bz)_6(MeOH)_4]_n$ (**1a**) with the atomic numbering scheme for non-hydrogen atoms

Table 1. Selected bond lengths [Å] and bond angles [°] for complexes **1a**−**c**

1a		**1b**		**1c**	
Eu(1)···Eu(2)	4.90	Gd(1)···Gd(2)	4.89	Tb(1)···Tb(2)	4.88
Eu(1)···Eu(2*)	4.93	Gd(1)···Gd(2*)	4.92	Tb(1)···Tb(2*)	4.91
Eu(1)−O(2)	2.344(6)	Gd(1)−O(2)	2.326(6)	Tb(1)−O(2)	2.30(1)
Eu(1)−O(4)	2.320(6)	Gd(1)−O(4)	2.297(7)	Tb(1)−O(4)	2.30(1)
Eu(1)−O(5)	2.476(6)	Gd(1)−O(5)	2.506(7)	Tb(1)−O(5)	2.43(1)
Eu(1)−O(6)	2.510(6)	Gd(1)−O(6)	2.476(7)	Tb(1)−O(6)	2.48(1)
Eu(1)−O(7)	2.333(6)	Gd(1)−O(7)	2.355(7)	Tb(1)−O(7)	2.28(1)
Eu(1)−O(9)	2.309(6)	Gd(1)−O(9)	2.305(7)	Tb(1)−O(9)	2.29(1)
Eu(1)−O(13)	2.523(6)	Gd(1)−O(13)	2.516(7)	Tb(1)−O(13)	2.49(1)
Eu(1)−O(14)	2.496(6)	Gd(1)−O(14)	2.481(7)	Tb(1)−O(14)	2.46(1)
Eu(2)−O(1)	2.314(6)	Gd(2)−O(1)	2.377(7)	Tb(2)−O(1*)	2.28(1)
Eu(2)−O(3)	2.315(6)	Gd(2)−O(3)	2.336(7)	Tb(2)−O(3*)	2.29(1)
Eu(2)−O(8)	2.367(6)	Gd(2)−O(8)	2.316(6)	Tb(2)−O(8)	2.32(1)
Eu(2)−O(10)	2.348(6)	Gd(2)−O(10)	2.323(7)	Tb(2)−O(10)	2.32(1)
Eu(2)−O(11)	2.468(6)	Gd(2)−O(11)	2.491(8)	Tb(2)−O(11)	2.42(1)
Eu(2)−O(12)	2.527(6)	Gd(2)−O(12)	2.455(7)	Tb(2)−O(12)	2.48(1)
Eu(2)−O(15)	2.535(6)	Gd(2)−O(15)	2.494(7)	Tb(2)−O(15)	2.50(1)
Eu(2)−O(16)	2.507(6)	Gd(2)−O(16)	2.517(7)	Tb(2)−O(16)	2.49(1)
O(13)···O(11)	2.72	O(13)···O(12*)	2.74	O(13)···O(11)	2.73
O(14)···O(12*)	2.83	O(14)···O(11)	2.87	O(14)···O(12*)	2.88
O(15)···O(5*)	2.76	O(15)···O(5*)	2.83	O(15)···O(5*)	2.76
O(16)···O(6)	2.82	O(16)···O(6)	2.76	O(16)···O(6)	2.82
Eu(2*)−Eu(1)−Eu(2)	165.7	Gd(2*)−Gd(1)−Gd(2)	165.8	Tb(2*)−Tb(1)−Tb(2)	166.2

angle [Eu(1′)−Eu(1)−Eu(1*) = 158.4°], the carboxylate linked one-dimensional array can be best described as a linear chain. Intra-chain hydrogen bonding is observed between the doubly bridged Eu(1)···Eu(1′) unit, arising from a coordinated methanol H atom and carboxylate O atoms [O(8)−H(20)···O(1*) = 2.22 Å and O(8)−H(20)···O(7*) = 2.20 Å, respectively]. The single coordination mode may be accounted for by the presence of a bulky CF_3 group. This matches well with the results reported by Tahir et al.[20] for a cerium 3,5-dinitrobenzoate dihydrate complex $[Ce_2(C_7H_3N_2O_6)_6(H_2O)_4]_n$. The outer sphere in each repeating unit of $[Eu(cf_3)_3(MeOH)_2]$ contains one solvated methanol molecule. Two CF_3 groups of the ligands are disordered in the monomeric unit. Like those in complexes **1a**−**c**, the coor-

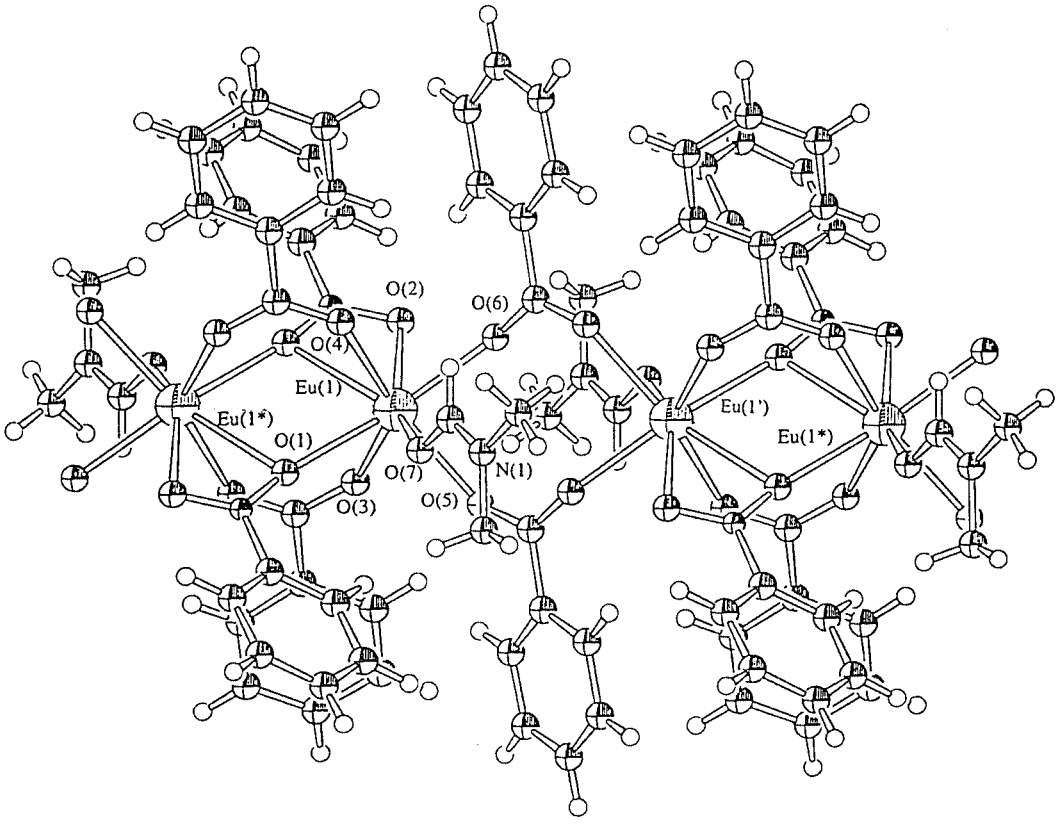

Figure 2. Polymeric structure of $[Eu(Bz)_3(DMF)]_n$ (**2a**) with the atomic numbering scheme for Eu and O atoms

Table 2. Selected bond lengths [Å] and bond angles [°] for complexes **2a−c**

2a		**2b**		**2c**	
Eu(1)···Eu(1*)	3.93	Gd(1)···Gd(1*)	3.91	Tb(1)···Tb(1*)	3.90
Eu(1)···Eu(1′)	5.34	Gd(1)···Gd(1′)	5.33	Tb(1)···Tb(1′)	5.33
Eu(1)−O(1)	2.333(3)	Gd(1)−O(1)	2.325(2)	Tb(1)−O(1)	2.30(2)
Eu(1)−O(1*)	2.580(3)	Gd(1)−O(1*)	2.579(2)	Tb(1)−O(1*)	2.52(2)
Eu(1)−O(2)	2.513(3)	Gd(1)−O(2*)	2.492(2)	Tb(1)−O(2*)	2.48(2)
Eu(1)−O(3)	2.403(3)	Gd(1)−O(3)	2.395(2)	Tb(1)−O(3)	2.38(2)
Eu(1)−O(4)	2.382(3)	Gd(1)−O(4)	2.371(2)	Tb(1)−O(4)	2.41(2)
Eu(1)−O(5)	2.354(3)	Gd(1)−O(5)	2.349(2)	Tb(1)−O(5)	2.28(2)
Eu(1)−O(6)	2.306(3)	Gd(1)−O(6)	2.299(2)	Tb(1)−O(6)	2.28(2)
Eu(1)−O(7)	2.422(3)	Gd(1)−O(7)	2.415(2)	Tb(1)−O(7)	2.31(2)
Eu(1′)−Eu(1)−Eu(1*)	169.5	Gd(1′)−Gd(1)−Gd(1*)	169.6	Tb(1′)−Tb(1)−Tb(1*)	169.6

dination polyhedron of complex **3a** can best be described as either a distorted square antiprism or a bicapped trigonal prism, with the dihedral angles between the corresponding planes being 3.78 and 7.10°, respectively. For the square antiprism geometry, the top square plane is defined by O(1), O(2), O(7), and O(8), and the bottom plane is completed by O(3), O(4*), O(5), and O(6). For the distorted bicapped trigonal geometry the top plane is formed by O(1), O(3), and O(5), and the bottom plane is composed of O(2), O(4*), and O(6), while the O(7) and O(8) atoms cap two quadrilateral faces of the trigonal prism. The Eu−O(CO) distances [2.360(5)−2.446(4) Å] and the Eu−O(MeOH) distances [2.521(5)−2.600(5) Å] are similar to those in complex **1a**. Table 3 summarises selected bond lengths and bond angles in complexes **3a** and **3c**.

The coordination geometry of the carboxylate ligands in complexes **4a−c** is similar to that in the lanthanide benzoate complexes **1a−c**. A perspective drawing of complex **4a** is illustrated in Figure 4, and selected bond lengths and bond angles are shown in Table 4. Each Eu^{3+} ion is connected to two neighbouring ones through four bridging carboxylate groups to form an infinite one-dimensional chain along the *a* axis. The coordination sphere is completed by a bidentate chelating carboxylate group and two

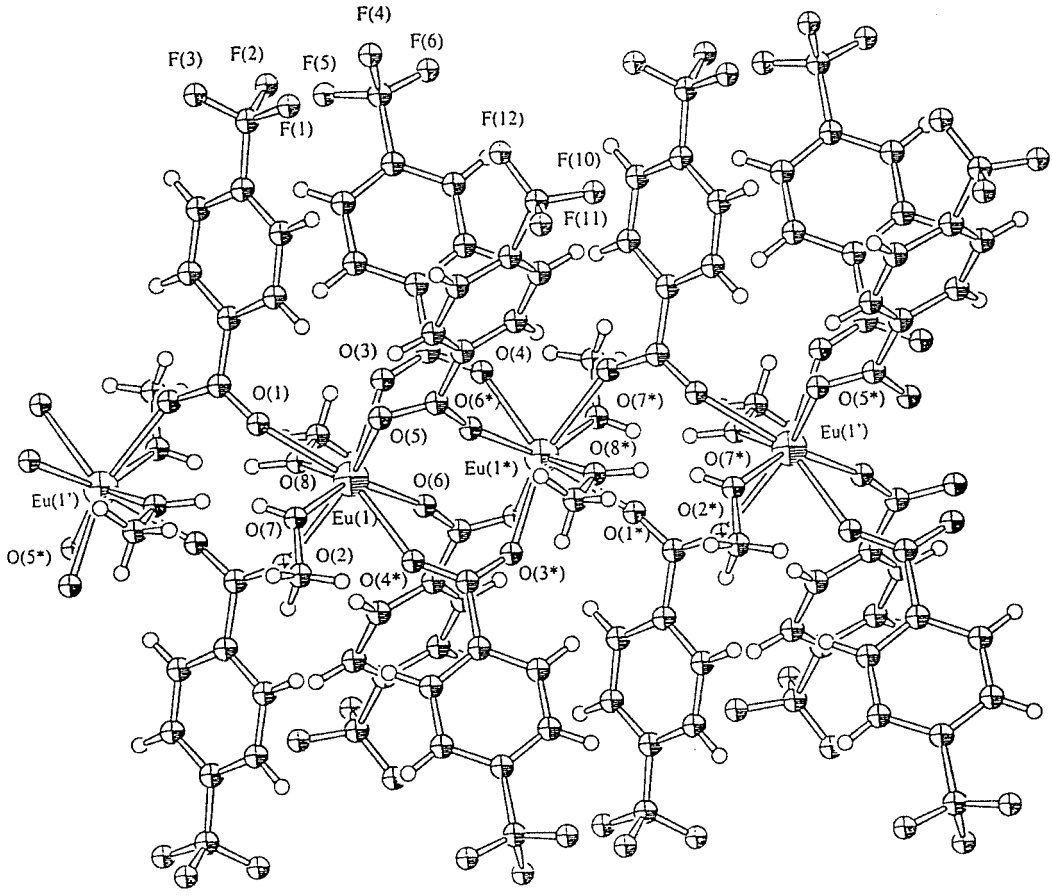

Figure 3. Polymeric structure of $[Eu(cf_3)_3(MeOH)_2]_n$ (**3a**) with the atomic numbering scheme for Eu, F and O atoms

Table 3. Selected bond lengths [Å] and bond angles [°] for complexes **3a** and **3c**

3a		**3c**	
Eu(1)−Eu(1*)	4.19	Tb(1)−Tb(1*)	4.21
Eu(1)−Eu(1′)	5.42	Tb(1)−Tb(1′)	5.37
Eu(1)−O(1)	2.362(4)	Tb(1)−O(1)	2.335(2)
Eu(1)−O(2)	2.378(4)	Tb(1)−O(2)	2.345(2)
Eu(1)−O(3)	2.363(4)	Tb(1)−O(3)	2.339(3)
Eu(1)−O(4*)	2.369(4)	Tb(1)−O(4*)	2.346(3)
Eu(1)−O(5)	2.446(4)	Tb(1)−O(5)	2.418(3)
Eu(1)−O(6)	2.360(5)	Tb(1)−O(6)	2.325(3)
Eu(1)−O(7)	2.600(5)	Tb(1)−O(7)	2.591(3)
Eu(1)−O(8)	2.521(5)	Tb(1)−O(8)	2.515(3)
O(8)−H(20)···O(1*)	2.22	O(8)−H(20)···O(1*)	2.27
O(8)−H(20)···O(7*)	2.20	O(8)−H(20)···O(7*)	2.30
Eu(1′)−Eu(1)−Eu(1*)	158.4	Tb(1′)−Tb(1)−Tb(1*)	159.1

methanol molecules. An intra-chain hydrogen bond between the coordinated methanol H atoms and chelating carboxylate O atoms is observed [O(10)−H(14)···O(5*) = 1.82 Å] and [O(11)−H(13)···O(4*) = 2.47 Å]. Along the infinite chain, the Eu···Eu distances in complex **4a** are alternatively long [Eu(1)···Eu(1′) = 5.03 Å] and short [Eu(1)···Eu(1*) = 4.86 Å]. With the alternating Eu···Eu distances and the chain angle [Eu(1′)−Eu(1)−Eu(1*) = 159.3°], the carboxylate-linked one-dimensional array can best be described as a linear chain. The difference between the alternating metal−metal distances is smaller than in complex **2a**, because the bridging unit in **4a** is made up of the same number of ligands and coordinating modes. However, this coordination geometry should not cause such a difference in the metal−metal distances along the chain. This can be explained by studying the molecular structure, in which the orientations of the carboxylate ligands align in the same direction in the alternating monomeric unit. Increased steric hindrance in that unit would result in a slightly longer metal−metal distance. Similarly to that in complex **3a**, the coordination geometry about the Eu(1) atom may be described either as a distorted square antiprism or as a bicapped trigonal prism. The square planes formed around the Eu(1) atom by O(1*)−O(2)−O(4)−O(11) and O(5)−O(7)−O(8)−O(10) adopt a distorted square antiprism geometry, with the dihedral angle between these planes being 11.74°. Meanwhile, the geometry of the distorted bicapped trigonal prism is made up of the top plane [O(1*)−O(4)−O(8)] and the bottom plane [O(2)−O(7)−O(11)], while the quadrilateral faces of the trigonal prism are capped by atoms O(5) and O(10). The dihedral angle between the planes is 16.46°. The

Eu−O(CO) bond lengths of the chelating and bridging carboxylate groups are 2.513(5)−2.532(7) Å and 2.296(6)−2.369(6) Å, respectively, while the Eu−O(MeOH) distances are 2.486(6) and 2.541(6) Å. These Eu−O bond lengths fall in the usual range of other known lanthanide carboxylates.[18a,18b]

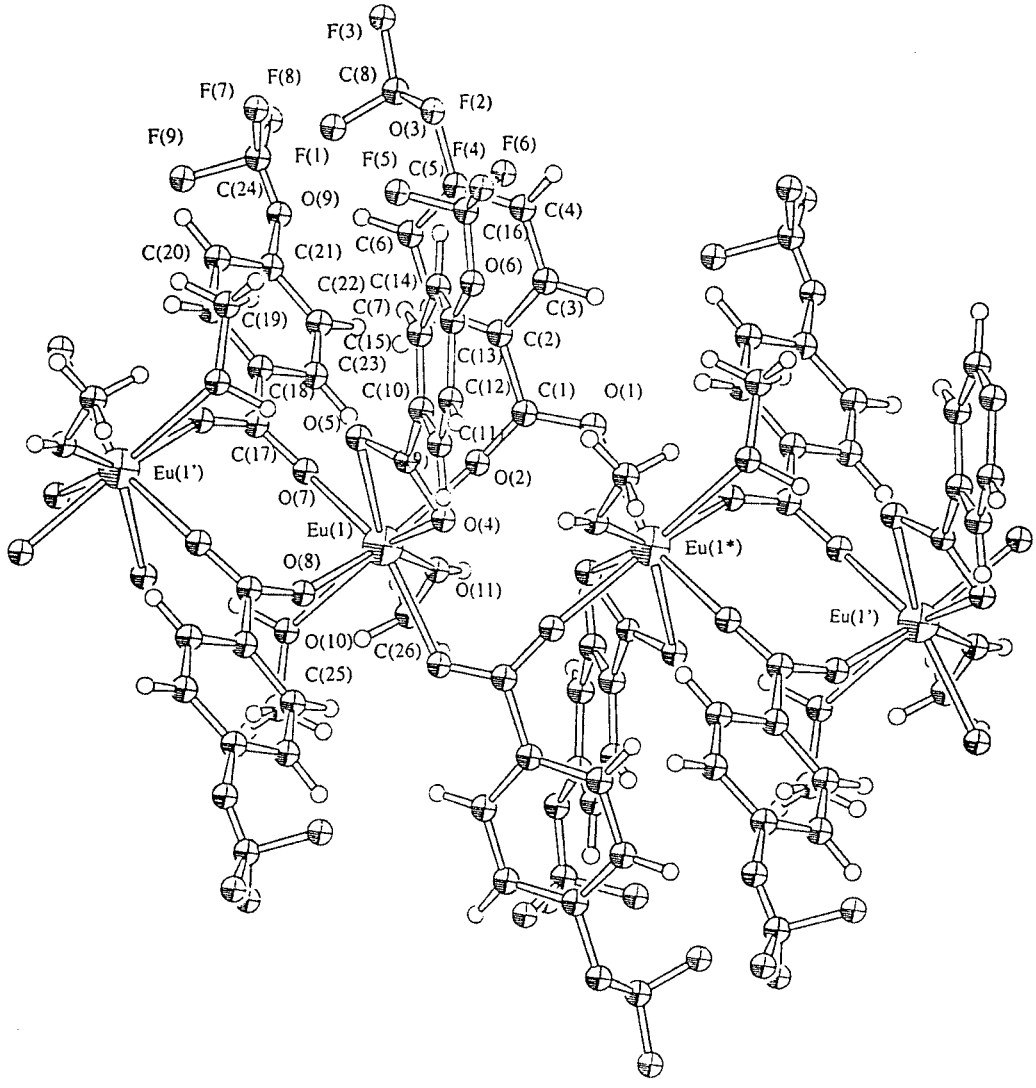

Figure 4. Polymeric structure of $[Eu(ocf_3)_3(MeOH)_2]_n$ (**4a**) with the atomic numbering scheme for non-hydrogen atoms

Table 4. Selected bond lengths [Å] and bond angles [°] for complexes **4a−c**

4a		**4b**		**4c**	
Eu(1)···Eu(1*)	4.86	Gd(1)···Gd(1*)	4.86	Tb(1)···Tb(1*)	4.79
Eu(1)···Eu(1′)	5.03	Gd(1)···Gd(1′)	5.00	Tb(1)···Tb(1′)	5.05
Eu(1)−O(1*)	2.369(6)	Gd(1)−O(1)	2.326(4)	Tb(1)−O(1)	2.394(3)
Eu(1)−O(2)	2.337(6)	Gd(1)−O(2*)	2.341(4)	Tb(1)−O(2*)	2.229(3)
Eu(1)−O(4)	2.532(7)	Gd(1)−O(4)	2.526(4)	Tb(1)−O(4)	2.363(3)
Eu(1)−O(5)	2.513(5)	Gd(1)−O(5)	2.488(4)	Tb(1)−O(5)	2.925(3)
Eu(1)−O(7)	2.296(6)	Gd(1)−O(7)	2.311(4)	Tb(1)−O(7)	2.025(3)
Eu(1)−O(8)	2.319(6)	Gd(1)−O(8*)	2.289(5)	Tb(1)−O(8)	2.621(3)
Eu(1)−O(10)	2.541(6)	Gd(1)−O(10)	2.503(4)	Tb(1)−O(10)	2.236(4)
Eu(1)−O(11)	2.486(6)	Gd(1)−O(11)	2.475(5)	Tb(1)−O(11)	2.757(4)
O(10)−H(14)···O(5*)	1.82	O(10)−H(19)···O(5*)	1.87	O(10)−H(20)···O(5*)	2.23
O(11)−H(13)···O(4*)	2.47	O(11)−H(20)···O(4*)	1.85	O(11)−H(13)···O(4*)	1.86
Eu(1′)−Eu(1)−Eu(1*)	159.3	Gd(1′)−Gd(1)−Gd(1*)	159.3	Tb(1′)−Tb(1)−Tb(1*)	159.0

The molecular structure of complex **5b** was established by X-ray crystallography, and the polymeric structure of the complex is depicted in Figure 5. Selected bond lengths are given in Table 5. The structure consists of an asymmetric dimer in which Gd^{3+} ions, in non-equivalent positions, are connected by two ligands through the carboxylate groups. These two carboxylate groups are bidentate bridging, and bind to two Gd^{3+} ions simultaneously. Each Gd^{3+} ion is further coordinated to two bidentate chelating carboxylate groups, one water molecule and one dimethylformamide (DMF) to form eight-coordinate metal ions. Furthermore, intramolecular hydrogen bonding interaction links the two Gd^{3+} ions through the coordinated water H atom and carboxylate O atom of the ligands [O(21)−H(72)···O(13) = 2.35 Å and O(22)−H(70)···O(2) = 1.75 Å]. The Gd···Gd distance is 4.46 Å, longer than that in the Gd^{3+} complex $[Gd(C_3H_5O_2)_3(H_2O)_2]_2{\cdot}4H_2O{\cdot}2(CH_4N_2S)$[21] because of the larger steric effect from the ethoxybenzoate ligand. The coordination polyhedron of the Gd(1) atom can be described either as a distorted bicapped trigonal prism or as a square antiprism. In the bicapped trigonal prism description, the top plane is formed by O(2), O(4), and O(7), and the bottom plane is completed by O(10), O(19), and O(21), while the quadrilateral faces of the trigonal prism [O(2)−O(4)−O(10)−O(19) and O(4)−O(7)−O(19)−O(21)] are capped by O(1) and O(5), respectively. The dihedral angle between the trigonal faces is 5.50°. Besides this description, it can also be treated as a distorted square antiprism. One square face is defined by O(1), O(4), O(5), and O(19), whereas the other face is completed by O(2), O(7), O(10), and O(21). The dihedral angle between the square faces is 7.60° and the Gd(1)−O bond lengths range from 2.333(5) to 2.541(5) Å. The Gd(1)−O distances for the chelating carboxylate groups [2.414(5)−2.541(5) Å] are significantly longer than those of the bridging carboxylate groups [2.333(5)−2.359(6) Å], since lengthening of the chelating carboxylate group is caused by the formation of an unstable four-membered chelate ring with the Gd^{3+} ion. In addition,

Table 5. Selected bond lengths [Å] for complexes **5a** and **5b**

5a		**5b**	
Gd(1)···Gd(2)	4.46	Tb(1)···Tb(2)	4.50
Gd(1)−O(1)	2.463(5)	Tb(1)−O(1)	2.444(5)
Gd(1)−O(2)	2.414(5)	Tb(1)−O(2)	2.427(4)
Gd(1)−O(4)	2.422(5)	Tb(1)−O(4)	2.391(6)
Gd(1)−O(5)	2.541(5)	Tb(1)−O(5)	2.511(5)
Gd(1)−O(7)	2.359(6)	Tb(1)−O(7)	2.341(6)
Gd(1)−O(10)	2.333(5)	Tb(1)−O(10)	2.320(5)
Gd(1)−O(19)	2.368(6)	Tb(1)−O(19)	2.310(6)
Gd(1)−O(21)	2.408(5)	Tb(1)−O(21)	2.395(5)
Gd(2)−O(8)	2.326(5)	Tb(2)−O(8)	2.283(6)
Gd(2)−O(11)	2.365(6)	Tb(2)−O(11)	2.340(6)
Gd(2)−O(13)	2.453(5)	Tb(2)−O(13)	2.447(6)
Gd(2)−O(14)	2.473(6)	Tb(2)−O(14)	2.406(4)
Gd(2)−O(16)	2.532(5)	Tb(2)−O(16)	2.530(5)
Gd(2)−O(17)	2.418(5)	Tb(2)−O(17)	2.394(6)
Gd(2)−O(20)	2.342(5)	Tb(2)−O(20)	2.378(5)
Gd(2)−O(22)	2.410(5)	Tb(2)−O(22)	2.395(5)
O(21)−H(72)···O(13)	2.35	O(21)−H(57)···O(14)	1.79
O(22)−H(70)···O(2)	1.75	O(22)−H(58)···O(2)	2.01

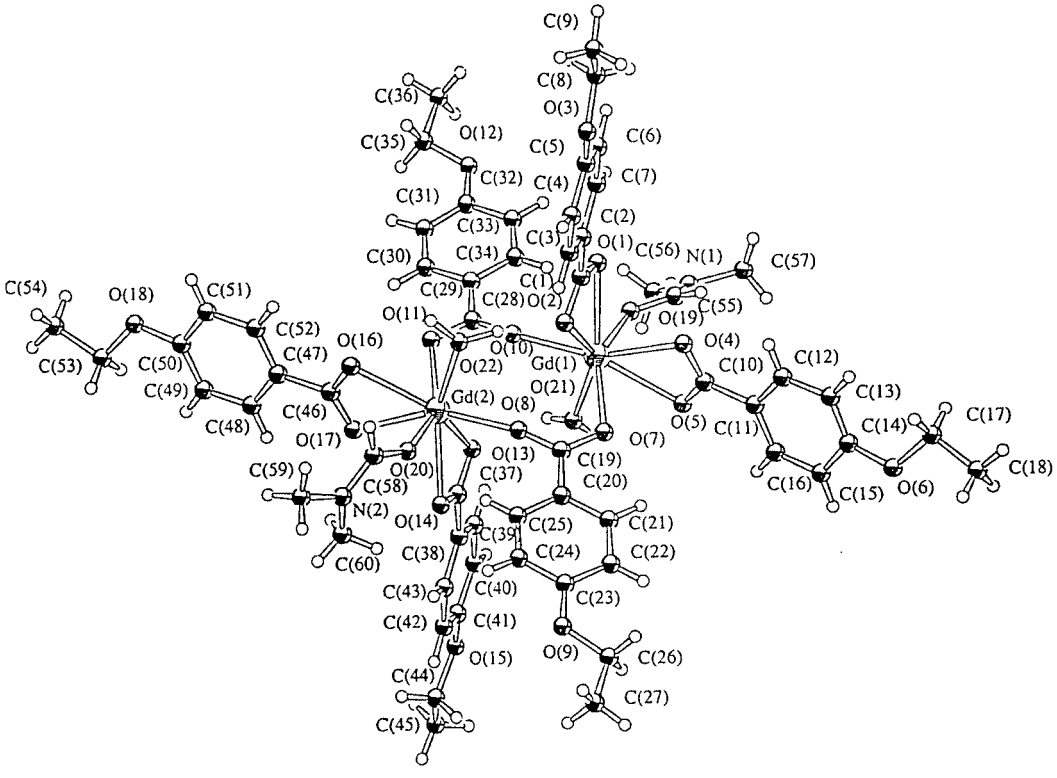

Figure 5. Molecular structure of $[Gd(oet)_3(DMF)(H_2O)]_2$ (**5b**) with the atomic numbering scheme for non-hydrogen atoms

the description of the coordination sphere around the Gd(2) atom is similar to that of Gd(1). The distorted bicapped trigonal prism consists of the top plane [O(11)−O(13)−O(17)] and the bottom plane [O(8)−O(20)−O(22)], with a dihedral angle of 5.74° between them. For the distorted square antiprism, the defining planes are made up by O(8)−O(11)−O(13)−O(22) and O(14)−O(16)−O(17)−O(20), with a dihedral angle of 6.25°. The Gd(2)−O distances [2.326(5)−2.532(5) Å] are close to the value of the Gd(1)−O distances, and the Gd(2)−O distances of chelating carboxylate [2.418(5)−2.532(5) Å] are longer than those of the bridging carboxylate [2.326(5)−2.365(6) Å], which are consistent with the Gd(1) values.

The molecular structure of complex **6c** is shown in Figure 6, and selected bond lengths and bond angles are tabulated in Table 6. The Tb^{3+} ion is connected to two neighbouring metal ions through four bidentate bridging carboxylate ligands to form an infinite chain along the *c* axis, and it is coordinated by eight oxygen atoms: four from carboxylate ligands, two from a nitrate ion and two from the methanol molecules. Along the chain, the Tb···Tb distance is 5.35 Å and the Tb(1*)−Tb(1)−Tb(1*) angle is 173.6°, and the structure of the complex can thus be de-

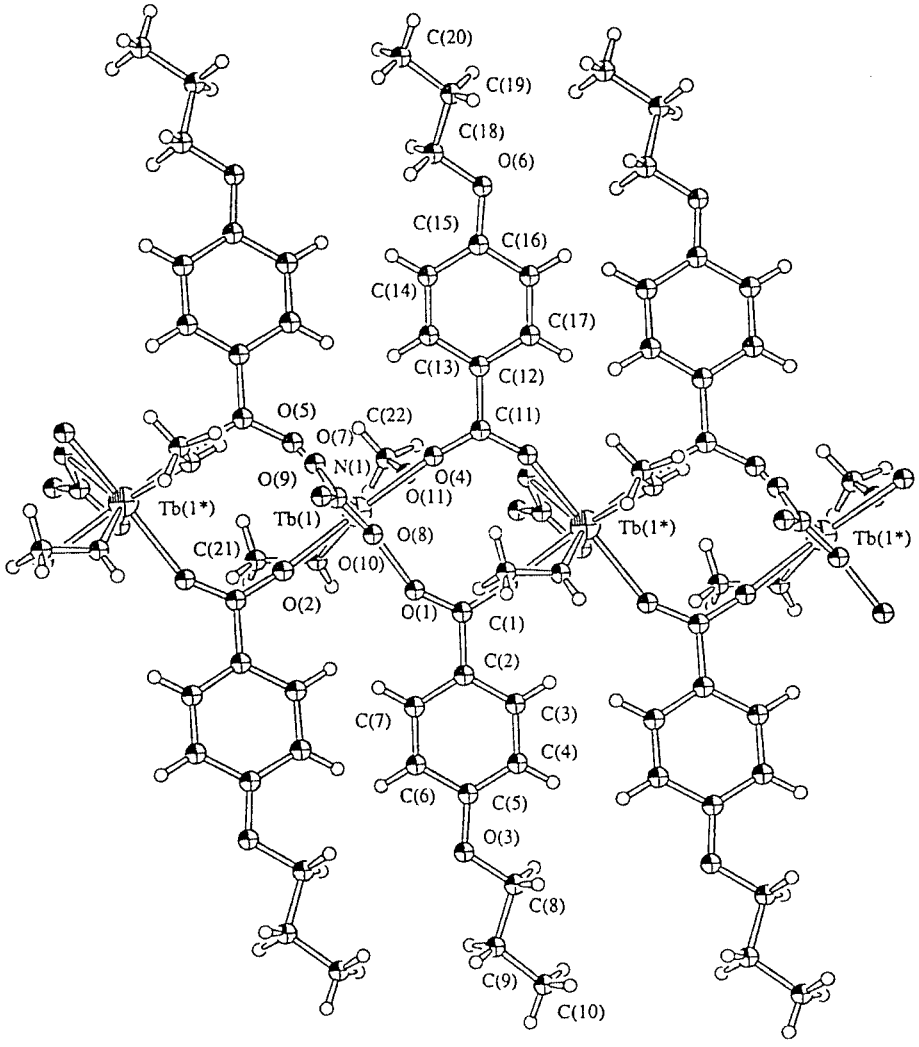

Figure 6. Molecular structure of $[Tb(opr)_2(NO_3)(MeOH)_2]_n$ (**6c**) with the atomic numbering scheme for non-hydrogen atoms

Table 6. Selected bond lengths [Å] and bond angles [°] for complex **6c**

			6c		
Tb(1)···Tb(1*)	5.35	Tb(1)−O(7)	2.521(4)	N(1)−O(8)	1.256(7)
Tb(1)−O(1)	2.273(4)	Tb(1)−O(8)	2.564(4)	N(1)−O(9)	1.234(7)
Tb(1)−O(2)	2.282(4)	Tb(1)−O(10)	2.413(4)	O(11)−H(30)···O(7*)	2.19
Tb(1)−O(4)	2.288(4)	Tb(1)−O(11)	2.474(4)		
Tb(1)−O(5)	2.277(4)	N(1)−O(7)	1.255(6)	Tb(1*)−Tb(1)−Tb(1*)	173.6

scribed as a linear chain skeleton. Intra-chain hydrogen bonding was observed between the coordinated methanol H atom and the O atom of the coordinated nitrate [O(11)−H(30)···O(7*) = 2.19 Å]. The coordination polyhedron around the Tb^{3+} ion can be described both as a distorted square antiprism and as a bicapped trigonal prism. It is hard to distinguish the polyhedron from these two typical coordination geometries, so both are illustrated here. For the distorted square antiprism geometry, the top square plane can be defined by O(1), O(2), O(8), and O(10), whereas the bottom plane is completed by O(4), O(5), O(7), and O(11). The dihedral angle between these two planes is 12.33°. For the distorted bicapped trigonal prism, on the other hand, the top plane is defined by O(1), O(4), and O(11), and the bottom plane is formed by O(2), O(5), and O(7), while O(8) and O(10) cap the quadrilateral faces of the trigonal prisms O(1)−O(2)−O(4)−O(7) and O(1)−O(2)−O(5)−O(11), respectively. The dihedral angle between the trigonal planes is 5.93°. The Tb−O(CO), Tb−O(NO_2), and Tb−O(MeOH) distances are 2.273(4)−2.288(4) Å, 2.521(4)−2.564(4) Å, and 2.413(4)−2.474(4) Å, respectively. The significant differences between the N−O bond lengths [1.234(7), 1.255(6), and 1.258(7) Å] indicate that the nitrate ion is bonded to the metal ion in a bidentate mode, as is evident from the IR spectra. Only two ligands are coordinated to the metal ion instead of the three in the previously described lanthanide carboxylates, and this is believed to be caused by steric hindrance by the propoxy groups, which prevents another ligand from coordinating to the metal to result in a longer metal−metal distance. An interesting feature of this complex is the propoxy groups on the benzoate ligands "bobbing up and down" along the chain.

Photophysical Properties

All complexes are soluble in hot MeOH or DMF solution, the improved solubility of the complexes being due to the *para*-substituted alkoxy and fluorinated groups. Consequently, the photophysical investigations were mainly carried out in MeOH solution, and solid-state luminescence was also studied.

Both the solid-state and the solution-state excitation spectra of the europium and terbium complexes match the corresponding electronic absorption profiles of the respective ligands throughout the UV spectral region, showing that ligand-to-metal energy transfer occurs. In addition, the absence of observable *f-f* absorption transitions in the excitation spectra reveals that the sensitisation process is favoured by indirect excitation. Excitation of the ligand-centred (LC) absorption bands results in the well-known narrow emission bands of the Eu^{3+} and Tb^{3+} ions, and their emission spectra are essentially identical in the solid state and in the solution state. Europium complex **1a** emits red light upon LC excitation, originating from the $^5D_0 \rightarrow {}^7F_n$ (n = 0, 1, 2, 3, 4) transitions, with the strongest emission due to the $^5D_0 \rightarrow {}^7F_2$ transition at 618 nm (Figure 7). The terbium complex **1c**, on the other hand, exhibits bright green luminescence in which the peaks in the emission spectrum correspond to the $^5D_4 \rightarrow {}^7F_n$ (n = 6, 5, 4, 3) transitions, with the strongest emission corresponding to the $^5D_4 \rightarrow {}^7F_5$ transition at 545 nm (Figure 8). Both of their time-resolved luminescence spectra show monoexponential decay, with luminescence lifetimes of 0.43 and 1.30 ms, respectively. A summary of the luminescent properties of the complexes is given in Table 7. The solid-state luminescent properties of both Eu and Tb benzoate complexes are similar to those reported by Wang[22] and Ronda,[23] in which the benzoate complexes have different structures. Degassed samples exhibit nearly identical luminescence observations and lifetime values, suggesting that oxygen quenching of the excited state can be neglected in this case. Although we have not been able to evaluate the efficiency of the energy transfer involved in these complexes quantitatively, there is an almost negligible emission intensity from the benzoate ligand, suggesting that the energy transfer process from ligand to metal is fairly efficient. This phenomenon is similar to those seen in other lanthanide benzoate complexes.[22−24]

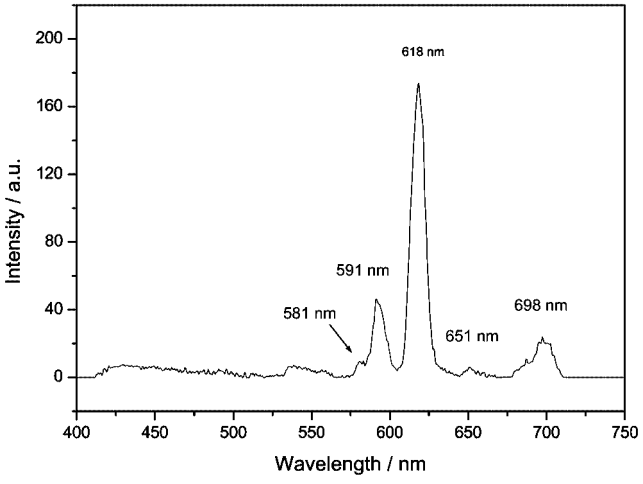

Figure 7. Emission spectrum of $[Eu_2(Bz)_6(MeOH)_4]_n$ (**1a**) in methanol at 298 K

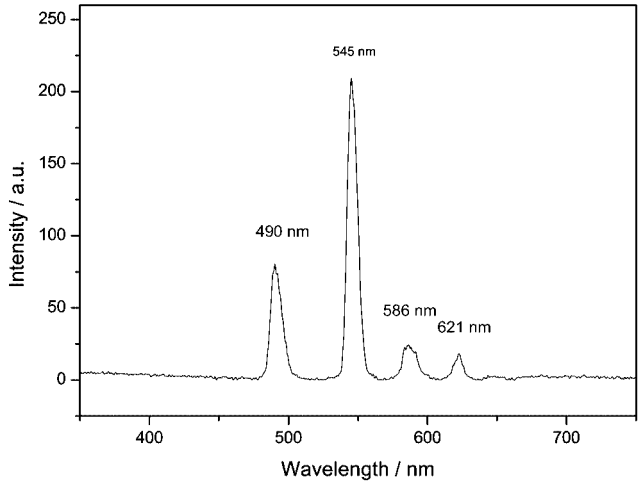

Figure 8. Emission spectrum of $[Tb_2(Bz)_6(MeOH)_4]_n$ (**1c**) in methanol at 298 K

Table 7. Luminescence lifetime of the europium and terbium carboxylate complexes measured in MeOH (τ_{MeOH}) and MeOD (τ_{MeOD}), as well as the number of coordinated solvent molecules (q) as determined by Horrocks' equation

Complex	τ_{MeOH} [ms]	τ_{MeOD} [ms]	q
1a	0.48	2.17	3.4±0.5
1c	1.30	1.59	1.2±0.5
3a	0.39	1.98	4.3±0.5
3c	0.98	1.21	1.6±0.5
4a	0.40	2.12	4.2±0.5
4c	0.90	1.12	1.8±0.5
6a	0.45	1.90	3.6±0.5
6c	1.03	1.36	2.0±0.5

The known sensitivity of Eu^{3+} and Tb^{3+} luminescence towards quenching by hydroxy groups in the solvent provides an experimental tool with which to estimate the degree of shielding by the ligands. An empirical relationship has been established by Horrocks and Sudnich,[25] estimating the number of coordinated methanol molecules (q) as $q = A(\tau_{MeOH}^{-1} - \tau_{MeOD}^{-1})$, where A is 2.1 for the Eu^{3+} and 8.4 for the Tb^{3+} complexes, and τ^{-1} is the reciprocal luminescence lifetime, measured separately in MeOH and in [D_4]methanol.

The luminescence lifetime of the complexes increases significantly in deuterated MeOH, indicating the quenching effect of the excited state of Ln^{3+} ions by the O−H oscillators of the coordinated methanol. The solvation parameter q determined is 3.4±0.5 and 1.2±0.5 for **1a** and **1c**, respectively (the error of ±0.5 is generally assumed to be reasonable for this calculation).[25b] This is consistent with three and one coordinated methanol molecule(s) in the first coordination sphere for the Eu^{3+} and Tb^{3+} ions. Additional contribution of solvent-based quenching from the second-sphere interaction may be considered. Parker et al.[26] have shown that significant lifetime differences can also be observed even when no solvent molecules are directly coordinated to the lanthanide ion. This is attributable to the contribution of second-sphere interaction and/or hydrogen bonding of solvent molecules to the ligand, giving rise to apparent q values of anywhere between 0 and 1.

Georges et al.[6a] reported the luminescent properties of terbium chelated with benzoic acid derivatives in aqueous solution, and suggested that, if the benzoic acid derivatives have similar triplet-state energy levels, sensitisation of the terbium luminescence is mainly determined by the ability of the acid to bind to the lanthanide ion. An electron-donating substituent group will increase the negative charge shift of the carboxylic carbon atom and hence also the stability constant of the complex. They also showed that the triplet-state energy levels of benzoic acid derivatives with *para*- and *ortho*-substituted OH and NH_2 groups are in the range of 23500−25500 cm^{-1}, which is above the emission level of $^5D_0$ for Eu^{3+} and $^5D_4$ for Tb^{3+} ions. This therefore supports the observation of stronger sensitisation of the terbium complexes than of the europium complexes, because of the smaller overlap between the ligand triplet and europium ion excited states. The above ligands' triplet state values can be used as a reference for our benzoate ligands and support the luminescent behaviour of the lanthanide complexes in our systems, in which stronger terbium emissions were observed.

The luminescence properties of lanthanide benzoate DMF complexes **2a** and **2c** display characteristic narrow-line emission bands, similar to those observed in complexes **1a** and **1c**, upon excitation of the LC absorption band at 277 nm in DMF and in the solid state. The reason for preparing these complexes with coordinated DMF molecules was to enhance the luminescence intensity and lifetime by eliminating the O−H oscillators that quenched the excited state of lanthanide ions from the coordinated methanol. Unfortunately, complexes **2a** and **2c** exhibit relatively weak luminescence upon LC excitation. This can be accounted for by the instability of the complexes in solution, arising from the possible association/dissociation process, since DMF is a strong O-donor solvent that may compete with the benzoate ligand to coordinate to the Ln^{3+} ions. The smaller antenna effect therefore results in lower sensitisation from the ligand to the metal ions, and thus lowers the luminescence intensity. Similar observation are made for complexes **5a** and **5c**.

Complexes **3a**, **3c**, **4a**, **4c**, **6a**, and **6c** show luminescent behaviour similar to that of complexes **1a** and **1b** in the solid state and in the solution state. Comparison of the lanthanide complexes with different benzoate ligands suggests that, according to their luminescent properties, electron-donating substituted groups such as ethoxy and propoxy increased the stability of the complexes, resulting in longer lifetimes and stronger intensities than seen for the benzoate lanthanides, while relatively shorter lifetimes were observed for electron-withdrawing groups such as trifluoromethyl and trifluoromethoxy. Concentrations of the complexes below 10^{-5} M result in changes of the excitation spectra as time passes, indicating that partial decomplexation occurs, which is understandable in view of the relatively weak coordination of bidentate carboxylate ligands. No attempts at quantum yield measurements were therefore made.

Magnetic Properties

The short metal−metal distance within the molecules demonstrated significant potential interest in terms of the study of the magnetic exchange interactions between those ions. We have previously reported the magnetic properties of the tetranuclear μ_4-oxo complexes, which exhibit antiferromagnetic coupling at low temperature.[27] From the evidence of the X-ray analyses of the complexes, they all have metal−metal distances (3.90−5.35 Å) believed to correspond to some magnetic interaction between the ions along the chain. Solid-state magnetic measurements were therefore carried out for the gadolinium and terbium complexes. Table 8 summarises the magnetic properties of these complexes.

The temperature dependence of the magnetic properties of the dimeric complexes **5b** and **5c** were investigated at 100

Table 8. Magnetic data of the gadolinium and terbium carboxylate complexes

Complex	$\chi_M T$ at 298 K [$cm^3 \cdot K \cdot mol^{-1}$]	$\chi_M T$ at 2 K [$cm^3 \cdot K \cdot mol^{-1}$]	Curie constant C [$cm^3 \cdot K \cdot mol^{-1}$]	Weiss constant θ [K]	J value [cm^{-1}]	g value
1b	17.04	15.55	16.97	−0.26	−0.021[a]	2.02[a]
1c	24.60	20.71	24.77	−4.62	−	−
2b	8.01	5.45	8.07	−1.09	−0.097[b]	1.97[b]
2c	12.10	4.07	12.24	−4.15	−	−
3b	7.89	7.88	7.91	0.14	−	−
3c	10.78	7.59	10.61	−1.65	−	−
4b	7.62	4.67	7.58	−1.91	−0.028[a]	1.95[a]
4c	11.56	8.54	11.77	−4.15	−	−
5b	15.86	10.74	15.48	−1.34	−0.068[b]	1.98[b]
5c	20.77	11.57	21.28	−10.50	−	−
6b	7.23	6.58	7.21	−0.58	−0.019[a]	1.92[a]
6c	10.5	8.94	10.70	−2.30	−	−

[a] Fitted by Equation (2). [b] Fitted by Equation (1).

Oe and 10 kOe field, respectively, over a temperature range of 2−300 K. Plots of χ_M^{-1} vs. T for these complexes obey the Curie−Weiss law, giving C = 15.48 and 21.28 $cm^3 \cdot K \cdot mol^{-1}$ and θ = −1.34 and −10.50 K for **5b** and **5c**, respectively. The $\chi_M T$ value (15.86 $cm^3 \cdot K \cdot mol^{-1}$) of complex **5b** remain almost constant − and close to the expected value of two non-interacting free Gd^{3+} ions − from 300 to 25 K.[28] A dramatic drop in value below 25 K to 10.74 $cm^3 \cdot K \cdot mol^{-1}$ at 2 K was observed (Figure 9). This feature is indicative of weak antiferromagnetic coupling between the Gd^{3+} ions in the molecule. We can analyse the data quantitatively by using the equation deduced from the isotropic spin Hamiltonian, $H = -JS_{Gd1}S_{Gd2}$, with the quantum numbers $S_{Gd1} = S_{Gd2} = 7/2$. Equation (1) is for the magnetic susceptibility of dimeric system[29] with $x = J/kT$ and N = Avogadro's number, β = Bohr magneton, k = Boltzmann constant.

$$\chi_M = \left(\frac{2N\beta^2 g^2}{kT}\right)\left(\frac{e^x + 5e^{3x} + 14e^{6x} + 30e^{10x} + 55e^{15x} + 91e^{21x} + 140e^{28x}}{1 + 3e^x + 5e^{3x} + 7e^{6x} + 9e^{10x} + 11e^{15x} + 13e^{21x} + 15e^{28x}}\right) \quad (1)$$

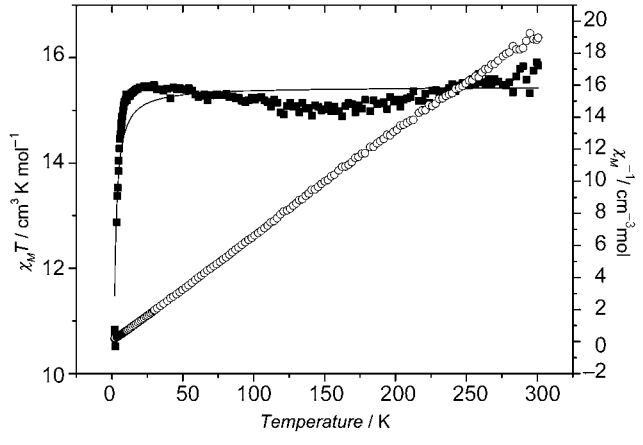

Figure 9. Temperature dependence of $\chi_M T$ (filled squares) and χ_M^{-1} (open circles) of $[Gd(oet)_3(DMF)(H_2O)]_2$ (**5b**) with diamagnetic correction; the solid line represents the best calculated curve

The magnetic interaction parameter J can be evaluated by fitting the data for the dimer system with Equation (1). The J value is −0.068 cm^{-1} whereas g is 1.98. A good agreement between the experimental and calculated values is reflected by the small R value [$R = \Sigma(\chi_M T_{calcd.} - \chi_M T_{obsd.})^2/\Sigma(\chi_M T_{obsd.})^2$] of $4.8 \cdot 10^{-4}$. Meanwhile, the $\chi_M T$ value of complex **5c** decreases gradually from room temperature (20.77 $cm^3 \cdot K \cdot mol^{-1}$) to 2 K (11.57 $cm^3 \cdot K \cdot mol^{-1}$). This room-temperature value is smaller than the expected values for two free non-interacting Tb^{3+} ions, which is primarily a consequence of the ligand field effect that the lowest J multiplet of the Russell−Saunders ground term was perturbed. The dramatic drop in $\chi_M T$ is mainly due to the splitting of the ligand field of the Tb^{3+} ions because of strong spin-orbit coupling, and partly contributed to the possible antiferromagnetic coupling between the Tb^{3+} ions in the dimer unit at a lower temperature.

A relatively longer metal−metal distance than seen in complexes **5b** and **5c** is associated with complex **6c** (5.35 Å). We believed such a large separation might give rise to some magnetic exchange behaviour, and so the solid-state magnetic properties of complexes **6b** and **6c** were studied over the 2−300 K temperature range, at 100 Oe applied field; χ_M is the molar magnetic susceptibility per monomer unit of the polymeric chain. For complex **6b**, the $\chi_M T$ value at room temperature is 7.23 $cm^3 \cdot K \cdot mol^{-1}$, close to the expected value for one isolated Gd^{3+} ion ($^8S_{7/2}$). However, the whole profile of the $\chi_M T$ vs. T plot is indicative of weak antiferromagnetic coupling, resulting in a nonmagnetic ground state for the Gd^{3+} ions. The abrupt drop of $\chi_M T$ at below 60 K, to the minimum value of 6.58 $cm^3 \cdot K \cdot mol^{-1}$, together with the negative θ value of −0.58 K, suggests the presence of weak antiferromagnetic coupling between the metal ions. As complex **6b** consists of an infinite chain with equal spacing, it can be quantitatively analysed by use of the equation deduced from the isotropic spin Hamiltonian, $H = -JS_{Gd1}S_{Gd2}$, with the quantum numbers $S_{Gd1} = S_{Gd2} = 7/2$. The analytical expression of Equation (2) for

the magnetic susceptibility of an infinite chain of classical spins was derived by Fisher[30] with

$$u = \coth\left[\frac{2JS(S+1)}{kT}\right] - \left[\frac{kT}{2JS(S+1)}\right]$$

and the other symbols as defined in Equation (1).

$$\chi_M = \frac{Ng^2\beta^2 S(S+1)}{3kT}\frac{1+u}{1-u} \quad (2)$$

A quantitative analysis of the data, based on Equation (2), shows a good fit of $\chi_M T$ with $J = -0.019$ cm^{-1}, $g = 1.92$ and $R = 1.17 \cdot 10^{-5}$. The magnetic behaviour of complex **6c** is similar to that of the Gd complex, indicating the possible presence of antiferromagnetic interaction between the Tb^{3+} ions. The data fit well with the Curie−Weiss law, with $C = 10.70$ cm^3 K·mol^{-1} and $\theta = -2.30$ K. The $\chi_M T$ value exhibits a continuous decrease upon cooling, from 10.5 cm^3·K·mol^{-1} at room temperature to 10.58 cm^3·K·mol^{-1} at ca. 130 K, and then drop very rapidly to 8.94 cm^3·K·mol^{-1} at 2 K. The continuous decrease in $\chi_M T$ as the temperature is lowered is probably primarily a result of the ligand field effect stemming from the strong spin-orbit coupling of the Tb^{3+} ions together with possible contribution from weak intra- and intermolecular antiferromagnetic coupling between the Tb^{3+} ions. The other complexes **1b**, **1c**, **2b**, **2c**, **3c**, **4b** and **4c**, but not **3b**, exhibit weak antiferromagnetic coupling between the lanthanide ions at low temperature, with behaviour similar to that of other homoleptic lanthanide complexes.[29,31]

Conclusion

A new series of lanthanide carboxylate complexes with benzoate-type ligands were successfully synthesised and demonstrated a rich coordination chemistry in the solid state. All benzoate ligands can sensitise lanthanide luminescence, especially for the terbium ion, but coordinated methanol molecules cause the quenching of lanthanide excited states. Although the use of *para*-substituted benzoate ligands improved the solubilities of the complexes, it gives rise to steric hindrance between the ligands, so that they have relatively shorter luminescence lifetimes than the complexes with benzoate ligands. Weak antiferromagnetic interactions between the neighbouring ions along the chain were observed at low temperature in studies of magnetic properties.

Experimental Section

General: All chemicals were purchased from commercial sources and were used as received without any further purification. The solid-state infrared spectra were recorded with a Bio-Rad FTS-7 FT-IR spectrometer on KBr pellets. Elemental analyses were performed by Butterworth Laboratories, UK. Thermal gravimetric analysis (TGA) was conducted with a Perkin−Elmer TGA 7 thermogravimetric analyser under nitrogen, over the 30−900 °C temperature range and with a heating rate of 20 °C/min. Electronic absorption spectra were recorded with a Hewlett Packard 8453 UV/Vis spectrophotometer at room temperature. Luminescence spectra were recorded with a Perkin−Elmer LS-50B luminescence spectrometer equipped with a Hamamatse R928 photomultiplier tube, with excitation and emission slit widths of 2.5−15 nm depending on the intensity of the emission. Solid samples were ground into fine powders prior to the luminescence measurements. Both aerated and deoxygenated solution luminescence spectra were measured at room temperature in the $1 \cdot 10^{-4}$ to $2 \cdot 10^{-5}$ M concentration range. For deoxygenated samples, the solutions were subjected to at least three freeze-pump-thaw cycles. Corrections were made for all excitation and emission spectra. Luminescence lifetimes, τ, were measured with the instrument in time-resolved mode, and are averages of at least three independent measurements made by monitoring the decay at a wavelength corresponding to the maximum intensity in the emission spectrum (618 nm for Eu and 545 nm for Tb), after pulsed excitation. The resulting first-order decay curve gave linear plots of ln(*Int*) vs. *t* from which the lifetime was calculated by $\tau = -1/\text{slope}$. Temperature-dependent magnetic susceptibilities of solid samples were recorded on a Quantum Design SQUID magnetometer (MPMS-5S) and a Oxford MagLab2000 magnetometer in the 2−300 K temperature range with applied fields of 100 Oe and 10000 Oe, respectively. The diamagnetic correction was estimated by use of Pascal's constants. Quantitative analyses of the magnetic susceptibility data for the complexes were performed by use of the Nonlin fitting program (Version 3.0).

Syntheses of the Lanthanide Complexes: Since the syntheses of the lanthanide complexes used similar procedures, the synthesis of complex **1a** is described as a general method. The respective ligands 4-(trifluoromethyl)benzoic acid, 4-(trifluoromethoxy)benzoic acid, 4-ethoxybenzoic acid, and 4-*n*-propoxybenzoic acid were used instead of benzoic acid for the preparation of complexes **2a**−**c**, **3a**−**c**, **4a**−**c**, **5a**−**c**, and **6a**−**c**.

General Method: Benzoic acid (82 mg, 0.672 mmol) and NaOH (26.9 mg, 0.672 mmol) in methanol (5 mL) were stirred at room temperature for 30 min. $Eu(NO_3)_3 \cdot 6H_2O$ (100 mg, 0.224 mmol) in methanol (2 mL) was added to the reaction mixture, and a white precipitate appeared after 1 d. The reaction mixture was further stirred for 12 h, and the precipitate was filtered and washed with methanol. **1a:** Yield: 202 mg, 78 %. IR (KBr disc): $\tilde{\nu}$ = 3527 br, 3450 br, 3072 m, 3060 m, 3029 w, 1593 s, 1539 vs, 1520 vs, 1428 vs, 714 s, 551 w cm^{-1}. ESI-MS (negative mode): *m*/*z* = 1152, 637. $C_{46}H_{46}Eu_2O_{16}$ (1158.78): calcd. C 47.68, H 4.00; found C 47.6, H 4.0. **1b:** Yield: 195 mg, 75 %. IR (KBr disc): $\tilde{\nu}$ = 3530 br, 3445 br, 3071 m, 3055 m, 3027 w, 1593 s, 1543 vs, 1522 vs, 1429 vs, 715 s, 553 w cm^{-1}. ESI-MS (negative mode): *m*/*z* = 1162, 642. $C_{46}H_{46}Gd_2O_{16}$ (1169.36): calcd. C 47.25, H 3.97; found C 47.3, H 4.0. **1c:** Yield: 210 mg, 81 %. IR (KBr disc): $\tilde{\nu}$ = 3528 br, 3449 br, 3072 m, 3058 m, 3030 w, 1594 s, 1541 vs, 1521 vs, 1430 vs, 714 s, 554 w cm^{-1}. ESI-MS (negative mode): *m*/*z* = 1166, 644. $C_{46}H_{46}O_{16}Tb_2$ (1172.71): calcd. C 47.11, H 3.95; found C 47.3, H 3.9. The product was dissolved in hot methanol for crystallisation and colourless single crystals of **1a**−**c** were obtained on slow evaporation of the solvent over a few days.

Complexes **2a**−**c** were prepared by dissolving complexes **1a**−**c**, respectively, in a minimum amount of hot dimethylformamide, colourless single crystals of **2a**−**c** being obtained after 2 d. **2a:** Yield: 80 mg, 61 %. IR (KBr disc): $\tilde{\nu}$ = 3065 m, 1661 s, 1603 s, 1558 s, 1527 s, 1446 m, 1422 s, 1399 s, 1374 m, 1107 w, 857 m, 723 s cm^{-1}. $C_{24}H_{22}EuNO_7$ (588.40): calcd. C 48.99, H 3.77, N 2.38; found C

49.0, H 3.7, N 2.4. **2b:** Yield: 76 mg, 58 %. IR (KBr disc): $\tilde{\nu}$ = 3060 m, 1658 s, 1603 s, 1559 s, 1530 s 1450 m, 1422 s, 1402 s, 1376 m, 1107 w, 855 m, 724 s cm^{-1}. $C_{24}H_{22}GdNO_7$ (593.69): calcd. C 48.55, H 3.74, N 2.36; found C 48.6, H 3.8, N 2.4. **2c:** Yield: 85 mg, 65 %. IR (KBr disc): $\tilde{\nu}$ = 3061 m, 1657 s, 1605 s, 1558 s, 1527 s 1448 m, 1423 s, 1400 s, 1375 m, 1107 w, 856 m, 723 s cm^{-1}. $C_{24}H_{22}NO_7Tb$ (595.37): calcd. C 48.42, H 3.72, N 2.35; found C 48.4, H 3.7, N 2.3.

The synthesis of complexes **3a**−**c** was similar to that described in the General Method. **3a:** Yield: 97 mg, 55 %. IR (KBr disc): $\tilde{\nu}$ = 3503 br, 3389 br, 3183 w, 3067 w, 1595 s, 1543 s, 1527 s, 1431 s, 1329 s, 1163 m, 1118 s, 1066 s, 1020 m, 868 m, 789 s, 709 m, 490 m cm^{-1}. ESI-MS (negative mode): *m*/*z* = 1628, 908. $C_{26}H_{20}EuF_9O_8$ (783.38): calcd. C 39.86, H 2.57; found C 39.8, H 2.6. **3b:** Yield: 86 mg, 49 %. IR (KBr disc): $\tilde{\nu}$ = 3505 br, 3389 br, 3175 w, 3072 w, 1599 s, 1547 s, 1531 s, 1437 s, 1335 s, 1165 m, 1118 s, 1068 s, 1018 m, 868 m, 789 s, 711 m, 490 m cm^{-1}. ESI-MS (negative mode): *m*/*z* = 1638, 914. $C_{26}H_{20}F_9Gd_8O$ (788.67): calcd. C 39.60, H 2.56; found C 39.6, H 2.5. **3c:** Yield: 105 mg, 60 %. IR (KBr disc): $\tilde{\nu}$ = 3503 br, 3393 br, 3185 w, 3073 w, 1597 s, 1551 s, 1531 s, 1435 s, 1333 s, 1165 m, 1118 s, 1068 s, 1018 m, 870 m, 791 s, 711 m, 490 m cm^{-1}. ESI-MS (negative mode): *m*/*z* = 1642, 915. $C_{26}H_{20}F_9O_8Tb$ (790.34): calcd. C 39.51, H 2.55; found C 39.6, H 2.6. Colourless block-shaped single crystals of **3a** and **3c** were obtained from the filtrate on slow evaporation of the solvent for 3 d.

The synthesis of complexes **4a**−**c** was similar to that described in the General Method. **4a:** Yield: 110 mg, 59 %. IR (KBr disc): $\tilde{\nu}$ = 3447 br, 1601 s, 1559 s, 1541 s, 1437 s, 1319 s, 1288 s, 1206 s, 1167 s, 783 m cm^{-1}. ESI-MS (negative mode): *m*/*z* = 1740, 972. $C_{26}H_{20}EuF_9O_{11}$ (831.38): calcd. C 37.56, H 2.42; found C 37.5, H 2.5. **4b:** Yield: 117 mg, 63 %. IR (KBr disc): $\tilde{\nu}$ = 3437 br, 1605 s, 1560 s, 1545 s, 1437 s, 1313 s, 1286 s, 1209 s, 1169 s, 783 m cm^{-1}. ESI-MS (negative mode): *m*/*z* = 1750, 978. $C_{26}H_{20}F_9GdO_{11}$ (836.67): calcd. C 37.32, H 2.41; found C 37.3, H 2.4. **4c:** Yield: 119 mg, 65 %. IR (KBr disc): $\tilde{\nu}$ = 3420 br, 1605 s, 1557 s, 1541 s, 1433 s, 1311 s, 1279 s, 1211 s, 1167 s, 783 m cm^{-1}. ESI-MS (negative mode): *m*/*z* = 1754, 979. $C_{26}H_{20}F_9O_{11}Tb$ (838.35): calcd. C 37.25, H 2.40; found C 37.3, H 2.4. Colourless rod-shaped single crystals of **4a**−**c** were obtained from the filtrate on slow evaporation of solvent for a week.

The synthesis of complexes **5a**−**c** was similar to that described in the General Method. **5a:** Yield: 182 mg, 55%. IR (KBr disc): $\tilde{\nu}$ = 3003 w, 2978 m, 2935 m, 2887 m, 1660 s, 1609 s, 1589 s, 1558 s, 1522 s, 1437 m, 1421 s, 1389 m, 1255 s, 784 w cm^{-1}. ESI-MS (−ve): *m*/*z* = 1460, 813. $C_{60}H_{72}Eu_2N_2O_{22}$ (1477.14): calcd. C 48.79, H 4.91, N 1.90; found C 48.8, H 5.0, N 1.9. **5b:** Yield: 172 mg, 52%. IR (KBr disc): $\tilde{\nu}$ = 3005 w, 2979 m, 2934 m, 2890 m, 1659 s, 1610 s, 1588 s, 1557 s, 1524 s, 1440 m, 1420 s, 1388 m, 1253 s, 783 w cm^{-1}. ESI-MS (negative mode): *m*/*z* = 1471, 818. $C_{60}H_{72}Gd_2N_2O_{22}$ (1487.73): calcd. C 48.44, H 4.88, N 1.88; found C 48.5, H 5.0, N 1.9. **5c:** Yield: 187 mg, 57%. IR (KBr disc): $\tilde{\nu}$ = 3003 w, 2978 m, 2934 m, 2888 m, 1659 s, 1607 s, 1589 s, 1558 s, 1524 s, 1439 m, 1419 s, 1389 m, 1255 s, 783 w cm^{-1}. ESI-MS (negative mode): *m*/*z* = 1474, 820. $C_{60}H_{72}N_2O_{22}Tb_2$ (1491.08): calcd. C 48.33, H 4.87, N 1.88; found C 48.4, H 4.9, N 1.9. Recrystallisation of the products from hot DMF afforded colourless rod-shaped single crystals of **5b** and **5c** after a few weeks.

The synthesis of complexes **6a**−**c** was similar to that described in the General Method. **6a:** Yield: 103 mg, 72 %. IR (KBr disc): $\tilde{\nu}$ = 3405 br, 3079 w, 2966 m, 2938 m, 2878 m, 1607 s, 1522 m, 1507 s, 1421 s, 1388 s, 1312 m, 1257 s, 1171 m, 786 w cm^{-1}. ESI-MS (negative mode): *m*/*z* = 1558, 869. $C_{22}H_{30}EuNO_{11}$ (636.44): calcd. C 41.52, H 4.75, N 2.20; found C 41.6, H 4.8, N 2.3. **6b:** Yield: 115 mg, 81%. IR (KBr disc): $\tilde{\nu}$ = 3406 br, 3079 w, 2965 m, 2938 m, 2878 m, 1607 s, 1522 m, 1508 s, 1421 s, 1389 s, 1311 m, 1257 s, 1173 m, 787 w cm^{-1}. ESI-MS (negative mode): *m*/*z* = 1569, 874. $C_{22}H_{30}GdNO_{11}$ (641.72): calcd. C 41.18, H 4.71, N 2.18; found C 41.2, H 4.8, N 2.2. **6c:** Yield: 128 mg, 90%. IR (KBr disc): $\tilde{\nu}$ = 3416 br, 3082 w, 2967 m, 2938 m, 2876 m, 1609 s, 1524 m, 1506 s, 1419 s, 1385 s, 1314 m, 1257 s, 1171 m, 787 w cm^{-1}. ESI-MS (negative mode): *m*/*z* = 1572, 875. $C_{22}H_{30}NO_{11}Tb$ (642.40): calcd. C 41.07, H 4.70, N 2.18; found C 41.1, H 4.7, N 2.2. A mixture of 4-*n*-propoxybenzoic acid, NaOH and $Tb(NO_3)_3{\cdot}6H_2O$ was left standing at room temperature, and colourless rod-shaped single crystals of **6c** were obtained on slow evaporation of the solvent for a few days.

Crystallography: Single crystals suitable for X-ray crystallographic analyses were mounted on sealed glass capillaries by use of epoxy resin. Diffraction data were collected at ambient temperature with a Rigaku AFC7R diffractometer, a Marresearch Image Plate Scanner or a Bruker AXS SMART-CCD 1000 diffractometer by use of graphite-monochromated Mo-K_α radiation (λ = 0.71073 Å) with ω-2θ and ω scan techniques. A summary of crystallographic data and structure refinements is listed in the Supporting Infornmation. All data sets were collected for Lorentz and polarisation effects and the absorption corrections based on ψ-scan methods[32] or inter-image scaling were also applied. All structures were solved by a combination of Patterson methods (DIRDIF92, PATTY)[33] or direct methods (SIR92[34] or SHELXS-86[35]) and difference Fourier techniques. The solutions were refined on *F* by full-matrix, least-squares analysis, with all metal and non-hydrogen atoms refined anisotropically for structures **2a**−**b**, **3c**, **4a**−**c**, and **6c**, while structures **1a**−**c**, **2c**, **3a**, **5b**, and **5c** were refined anisotropically for all metal and heavy atoms. All hydrogen atoms were included in the structure factor calculations but were not refined. All calculations were performed with a Silicon-Graphics workstation with the aid of the program package TeXsan.[36] CCDC-195568 to -195581 contain the supplementary crystallographic data for this paper. These data can be obtained free of charge at www.ccdc.cam.ac.uk/conts/retrieving.html or from the Cambridge Crystallographic Data Centre, 12, Union Road, Cambridge CB2 1EZ, UK [Fax: (internat.) + 44-1223/336-033; E-mail: deposit@ccdc.cam.ac.uk].

Supporting Information: A summary of crystallographic data, including the data collection and structure solution parameters for complexes **1a**−**c**, **2a**−**c**, **3a**, **3c**, **4a**−**c**, **5b**−**c** and **6c** is shown in Table S1. Magnetic data of complexes **5c**, **6b** and **6c** are illustrated in Figures S1−3, respectively (see also footnote on the first page of this article).

Acknowledgments

We gratefully acknowledge financial support from the Hong Kong Research Grants Council and the University of Hong Kong. A. W.-H. L. acknowledges the receipt of a postgraduate studentship and Hung Hing Ying scholarship administered by the University of Hong Kong. This work is partially supported by Hong Kong RGC (HKUST6157/00E) (X.-X. Z.).

[1] [1a] C. Galaup, C. Picard, B. Cathala, L. Cazaux, P. Tisnès, *Helv. Chim. Acta* **1999**, *82*, 543−560. [1b] N. Sabbatini, M. Guardigli, J.-M. Lehn, *Coord. Chem. Rev.* **1993**, *123*, 201−228. [1c] G. Blasse, G. J. Dirksen, N. Sabbatini, S. Perathoner, *Inorg. Chim. Acta* **1987**, *133*, 167−173.

[2] [2a] D. A. Bardwell, J. C. Jeffery, P. L. Jones, J. A. McCleverty, E. Psillakis, Z. Reeves, M. D. Ward, *J. Chem. Soc., Dalton Trans.* **1997**, 2079−2086. [2b] P. L. Jones, A. J. Amoroso, J. C. Jeffery, J. A. McCleverty, E. Psillakis, L. H. Ree, M. D. Ward, *Inorg. Chem.* **1997**, *36*, 10−18.

[3] [3a] L. Prodi, S. Pivari, F. Bolletta, M. Hissler, R. Ziessel, *Eur. J. Inorg. Chem.* **1998**, 1959−1965. [3b] J.-C. G. Bünzli, P. Froidevaux, J. M. Harrowfield, *Inorg. Chem.* **1993**, *32*, 3306−3311.

[4] [4a] A. Beeby, R. S. Dickins, S. Faulkner, D. Parker, J. A. G. Williams, *Chem. Commun.* **1997**, 1401−1402. [4b] A. Beeby, S. Faulkner, *Chem. Phys. Lett.* **1997**, *266*, 116−122. [4c] D. Parker, P. Kanthi-Senanayake, J. A. G. Williams, *J. Chem. Soc., Perkin Trans. 2* **1998**, 2129−2139.

[5] [5a] E. J. Nassar, P. S. Calefi, I. L. V. Rosa, O. A. Serra, *J. Alloys Comp.* **1998**, *275−255*, 838−840. [5b] J.-C. G. Bünzli, F. Ihringer, *Inorg. Chim. Acta* **1996**, *246*, 195−205. [5c] P. K. Sharma, A. R. van Doorn, A. G. J. Staring, *J. Lumin.* **1994**, *62*, 219−225.

[6] [6a] N. Arnaud, J. Georges, *Analyst* **2000**, *125*, 1487−1490. [6b] S. T. Mullins, P. G. Sammes, R. M. West, G. Yahioglu, *J. Chem. Soc., Perkin Trans. 1* **1996**, 75−81. [6c] J. B. Lamture, Z. H. Zhou, A. S. Kumar, T. G. Wensel, *Inorg. Chem.* **1995**, *34*, 864−869. [6d] G.F. de Sá, L. H. A. Nunes, Z.-M. Wang, G. R. Choppin, *J. Alloys Comp.* **1993**, *196*, 17−23.

[7] [7a] M. P. Oude Wolbers, F. C. J. M. Van Veggel, B. H. M. Snellink-Ruel, J. W. Hofstraat, F. A. J. Geurts, D. N. Reinhoudt, *J. Chem. Soc., Perkin Trans. 2* **1998**, 2141−2150. [7b] S. Petoud, J.-C. G. Bunzli, K. J. Schenk, C. Piguet, *Inorg. Chem.* **1997**, *36*, 1345−1353.

[8] W. W. Horrocks De Jr., P. Bolender, W. D. Smith, R. M. Supkowski, *J. Am. Chem. Soc.* **1997**, *119*, 5972−5973.

[9] [9a] I. Hemmilä, *J. Alloys Comp.* **1995**, *225*, 480−485. [9b] J. Coates, P. G. Sammes, G. Yahioglu, R. M. West, A. J. Garman, *J. Chem. Soc., Chem. Commun.* **1994**, 2311−2312. [9c] I. Hemmilä, *Applications of Fluorescence in Immunoassays*, Wiley, New York, **1991**.

[10] J. Kido, W. Ikeda, M. Kimura, K. Nagai, *Jpn. J. Appl. Phys.* **1996**, *35*, 394−396.

[11] [11a] J. P. Costes, J. M. Clemente-Juan, F. Dahan, F. Nicodme, M. Verelst, *Angew. Chem. Int. Ed.* **2002**, *41*, 323−325. [11b] A. Ouchi, Y. Suzuki, Y. Ohku, Y. Koizumi, *Coord. Chem. Rev.* **1988**, *92*, 29−43. [11c] R. C. Mehrotra, R. Bohra, *Metal Carboxylates*, Acad. Press, London, U.K., **1983**.

[12] [12a] G. Yu, Y. Q. Liu, X. Wu, D. B. Zhu, H. Y. Li, L. P. Jin, M. Z. Wang, *Chem. Mater.* **2000**, *12*, 2537−2541. [12b] S. Capecchi, O. Renault, D.-G. Moon, M. Halim, M. Etchells, P. J. Dobson, O. V. Salata, V. Christou, *Adv. Mater.* **2000**, *12*, 1591−1594. [12c] W. L. Li, Z. Q. Gao, Z. Y. Hong, C. S. Lee, S. T. Lee, *Synth. Met.* **2000**, *111−112*, 53−56. [12d] J. Kido, K. Nagai, Y. Okamoto, *J. Alloys Comp.* **1993**, *192*, 30−33.

[13] [13a] J. Kido, K. Nagai, Y. Okamoto, T. Skotheim, *Chem. Lett.* **1991**, *235*, 1267−1270. [13b] J. Kido, K. Nagai, Y. Ohashi, *Chem. Lett.* **1990**, *220*, 657−660.

[14] Y. X. Zheng, C. Y. Shi, Y. J. Liang, Q. Lin, C. Guo, H. J. Zhang, *Synth. Met.* **2000**, *114*, 321−323.

[15] A. Edward, C. Claude, I. Sokolik, T. Y. Chu, Y. Okamoto, R. Dorsinville, *J. Appl. Phys.* **1997**, *82*, 1841−1846.

[16] J. F. Ma, Z. S. Jin, J. Z. Ni, *J. Struct. Chem.* **1991**, *10*, 56−59.

[17] X. Li, X. Zheng, L. Jin, S. Lu, J. Zhang, *J. Mol. Struct.* **2001**, *559*, 341−346.

[18] [18a] G. Yang, H. A. Chen, Z. Y. Zhou, X. M. Chen, *J. Chem. Crystallogr.* **1999**, *29*, 309−317. [18b] E. Huskowska, I. Turowska-Tyrk, J. Legandziewicz, T. Glowiak, *J. Alloys Comp.* **1998**, *275*, 852−858. [18c] T. Imai, M. Shimoi, A. Ouchi, *Bull. Chem. Soc. Jpn.* **1987**, *60*, 159−167. [18d] Y. Sugita, A. Ouchi, *Bull. Chem. Soc. Jpn.* **1987**, *60*, 171−178.

[19] P. P. Gawryszewska, L. Jerrykiewicz, P. Sobota, J. Legendziewicz, *J. Alloys Comp.* **2000**, *300/301*, 275−282, references therein.

[20] M. N. Tahir, D. Ulku, C. Unaleroglu, E. M. Movsumov, *Acta Crystallogr., Sect. C* **1996**, *52*, 1449−1451.

[21] G. V. Romanenko, N. V. Podberezskaya, V. V. Bakakin, *Zh. Strukt. Khim.* **1981**, *22*, 185−188.

[22] C. Seward, N. X. Hu, S. N. Wang, *J. Chem. Soc., Dalton Trans.* **2001**, 134−137.

[23] M. Bredol, U. Kynast, C. Ronda, *Adv. Mater.* **1991**, *3*, 361−367.

[24] R. F. Wang, L. P. Jin, L. S. Li, S. Z. Lu, J. H. Zhang, *J. Coord. Chem.* **1999**, *47*, 279−287.

[25] [25a] R. C. Holz, C. A. Chang, W. D. Horrocks, *Inorg. Chem.* **1991**, *30*, 3270−3275. [25b] W. D. Horrocks, D. R. Sudnick, *Acc. Chem. Res.* **1981**, *14*, 384−392.

[26] S. Aime, M. Botta, D. Parker, J. A. G. Williams, *J. Chem. Soc., Dalton Trans.* **1996**, 17−20.

[27] A. W. H. Lam, W. T. Wong, G. H. Wen, X. X. Zhang, S. Gao, *New J. Chem.* **2001**, *25*, 531−533.

[28] [28a] E. A. Boundreaux, L. N. Mulay, *Theory and Applications of Molecular Paramagnetism*, J. Wiley & Sons: New York, **1976**. [28b] O. Kahn, *Molecular Magnetism*, VCH Publishers, New York, **1993**.

[29] A. Panagiotopoulos, T. F. Zafiropoulos, S. P. Perlepes, E. Bakalbassis, I. Masson-Ramade, O. Kahn, A. Terzis, C. P. Raptopoulou, *Inorg. Chem.* **1995**, *34*, 4918−4920.

[30] M. E. Fisher, *Am. J. Phys.* **1964**, *32*, 343−351.

[31] J. Legendziewicz, M. Borzechowska, G. Oezko, G. Meyer, *New J. Chem.* **2000**, *24*, 53−59.

[32] A. C. T. North, D. C. Phillips, F. S. Mathews, *Acta Crystallogr., Sect. A* **1968**, *24*, 351−359.

[33] P. T. Beursken, G. Admiraal, G. Beurskens, W. P. Bosman, S. Garcia-Granda, R. O. Gould, J. M. M. Smits, C. Smykalla, *The DIRDIF program system*, Technical Report of the Crystallography Laboratory, University of Nijmegen, The Netherlands, **1992**.

[34] *SIR92:* A. Altomare, M. C. Burla, M. Camalli, M. Cascarano, C. Giacovazzo, A. Guagliardi, G. Polidori, *J. Appl. Crystallogr.* **1994**, *27*, 435−436.

[35] *SHELXS 86*, Program for Crystal Structure Solution: G. M. Sheldrick, *Acta Crystallgr., Sect. A* **1990**, *46*, 467−473.

[36] *TeXsan:* Crystal Structure Analysis Package, Molecular Structure Corp., **1985** and **1992**.

Received July 4, 2002
[I02365]